Open access • Journal Article • DOI:10.1109/TGRS.1995.8746030

Polarized reflectance of bare soils and vegetation: measurements and models

François-Marie Bréon, Didier Tanré, P. Lecomte, Maurice Herman

Institutions: Centre national de la recherche scientifique

Published on: 01 Mar 1995 - IEEE Transactions on Geoscience and Remote Sensing (IEEE)

Topics: Specular reflection, Atmospheric correction, Backscatter and Optical polarization

Polarized Reflectance of Bare Soils and Vegetation: Measurements and Models

Francois-Marie Bréon, Didier Tanré, Pierre Lecomte and Maurice Herman

Abstract— **This paper presents a large set of spectral and directional signatures of the polarized reflectance acquired over various surfaces. Two analytical physically-based models were developed, one for bare soils and the other for simple vegetation cover. They consider that the polarized reflectance is generated by single specular reflection over isotropically distributed facets or leaves.**

The models accurately reproduce the order of magnitude and the directional signature of the reflectance for view angles of up to $\approx 55°$. It confirms that specular reflection is the main process that generates polarization over natural surfaces. Polarized light generated by other processes, and that are not accounted for by the models, can be observed however in the backscattering direction where single specular reflection does not yield polarization.

Although spectral variations in the polarized reflectance are observed, they are explained by atmospheric effects on the direct solar beam. The atmospheric correction yields a surface polarized reflectance which is larger than the model estimate, but is still on the same order of magnitude.

For the simple canopies studied, our results suggest that, except for particular events such as the "heading" of a canopy, vegetation will generate little variability in the polarized reflectance making this information unsuitable for monitoring of the canopies. On the other hand, since the models accurately predict the polarized reflectance from the surface, they can be used to correct airborne or spaceborne polarized reflectance measurements when the inversion of aerosol parameters is attempted.

I. Introduction

POLARIZED reflectance measurements of natural surfaces were initiated by [4]. Since then, there have been several attempts to correlate the polarized light reflected by surfaces to their biophysical properties. The polarization was said to be related to the surface roughness [44] and to the size of reflecting elements [15]. Some authors tried to correlate the polarization to soil moisture [5], [13] or to vegetation biomass [6]. It was also said that it could be used to produce a more accurate classification of surface cover [7], [15], [16] and estimation of vegetation canopy state [32], [41], [42]. A review of early attempts to use polarization for land surface remote sensing is given in [36]. Theoretical studies to understand the nature and to model the polarization from Earth surfaces were also performed: Polarization was thought to be generated by specular reflection at the surface of reflecting elements such as leaves [40], rocks or sand grains [23]. Reference [33] developed a physical model for vegetation canopies. The authors showed that the inversion of the model against field measurements allows an estimate of the canopy leaf angular distribution and so the estimation of the vegetation state. The polarization properties of natural targets have also been investigated in the laboratory using an incandescent lamp [43] or a polarized laser beam [20] as a source.

Despite these claims of the potentials of polarized light for the identification and characterisation of land surfaces, polarization measurement have not been used for global Earth monitoring. On the other hand, polarization has been used extensively in Astronomy research [29], for instance for a characterization of planets atmosphere with large optical thicknesses like those of Venus and Saturn [11], [12], [17], [24], [25], [27], [34], [35] or for studying the surface of Mars where the atmosphere is thin [14]. In the coming decade, two instruments will measure the polarization of Earth reflectances: the POLDER instrument (Polarization and Directionality of the Earth Reflectance; [9]) will be launched in 1996 on the Japanese ADEOS platform (Advanced Earth Observing Satellite). Similarly, the EOSP instrument (Earth Observing Scanning Radiometer; [39]) is scheduled on the AM2 platform of the EOS (Earth Observing System) program in 2003.

A major concern on the use of polarized light for the study of land surfaces is the capability to discriminate between polarization generated in the atmosphere [26] and that generated by the surface. In order to understand the relative order of magnitude of polarized light generated by the surface and the atmosphere, polarized measurements are needed over various ecosystems and for different atmospheric conditions. To achieve this objective, an airborne version of POLDER has been built and several field experiments already performed [2], [10], [21]. The airborne POLDER also acquired measurements during the HAPEX-Sahel experiment which was an international program focused on the soil-plant-atmosphere energy, water and carbon balances in the West African Sahel [22], [31]. In order to help the interpretation of the airborne measurements, a field instrument was also deployed and installed over various surfaces. The airborne measurements will be presented in a forthcoming paper and we here concentrate on the field measurements.

Manuscript received December 22, 1993; revised October 18, 1994. This work was supported in part by ORSTOM, Météo France, INSU/CNRS, Ministére de la Recherche et de l'Espace, Ministére de l'Environnement, Ministére de l'Education National et de la Culture and the Conseil Régional Midi-Pyréné es (all of France), ODA, NERC and the NERC TIGER Programme, JEP (all of the United Kingdom), NASA (USA), the European Community (grant N° EEC N-EPOC-CT90-0024-C (DSCN) and Environment EV5V-CT91-0033), and in part by several national funding agencies of Denmark, the Netherlands, and Germany.

F. M. Bréon is with LMCE/CEA, L'Orme des Merisiers 91191–Gif sur Yvette Cedex, France.

D. Tanré, P. Lecomte, and M. Herman are with LOA, Bat. P5, U.S.T. de Lille, URA CNRS 713, 59655–Villeneuve d'Ascq Cedex, France.

IEEE Log Number 9407847.

In this context, our objectives are 1) to present additional polarized reflectance measurements, including their directional signature, for various surface and atmosphere conditions; 2) to verify the hypothesis that polarized light is generated at the surface by specular reflection; 3) to design some simple models which accurately reproduce the measured polarization signatures; and 4) to investigate which surface parameters can be retrieved from the polarization signature.

In Section II, we recall general features of polarized light. Section III describes the field instrument and the measurement procedure. Two simple models for the polarized reflectance of vegetation and bare soils are described in Section IV. The results are presented in Section V. Section VI discusses the results in the context of spaceborne remote sensing and concludes.

II. Background

Polarized light can be described by the four Stokes parameters. In the Earth's atmosphere, the ellipticity of the radiance generated by natural processes has been shown to be negligible [28]. Thus, three parameters are sufficient to describe the state of the light. In this paper, we have normalized the measurements to the top of the atmosphere solar irradiance. The three parameters we use are then,

- ρ, the total reflectance which is the sum of unpolarized and polarized light,
- ρ_p which is the polarized portion of the total reflectance,
- and χ which is the angle of the linear polarization relative to the scattering plane (the plane which contains the solar and view directions).

Let us recall a few facts concerning polarized light:

Incoming solar light at the top of the atmosphere is unpolarized. Specular reflection polarizes light perpendicularly to the scattering plane ($\chi = 90°$). Similarly, Rayleigh single scattering polarizes light perpendicularly to the scattering plane. Single scattering by atmospheric aerosols generates light polarized either perpendicular ($\chi = 90°$) or in the plane of scattering ($\chi = 0°$). Multiple reflectance/scattering processes are necessary to yield a direction of polarization other than 0° or 90°. From symmetry considerations (assuming uniformity of the surface), light is always polarized either parallel or perpendicular to the principal plane. Thus, in those particular view directions, the *modified* polarized reflectance, defined as

$$\rho_{p\pm} = -\rho_p \cos(2\chi), \tag{1}$$

which can take positive or negative values, is sufficient to describe the state of polarization. $\rho_{p\pm}$ is positive (resp. negative) when polarization is perpendicular (resp. parallel) to the plane of scattering.

Most previously published works on polarization measurements use the degree of polarization as the variable of interest. The degree of polarization is the ratio of the polarized reflectance to the total reflectance ($P = \rho_p/\rho$). One major advantage of this parameter is its independence to the radiometer calibration and the incoming flux. On the other hand, this parameter ambiguously mixes the processes that generate unpolarized light, to those that generate polarized light, and so the degree of polarization is negatively correlated with the reflectance when the polarized reflectance is fairly constant. On the other hand, the polarized reflectance only accounts for those reflectance/scattering processes that generate polarized light. Therefore, in the present paper, we will consider this parameter, rather than the degree of polarization, as the parameter of interest.

III. Description of the Instrument and Methods

A. The Instrument

An instrument, called REFPOL, has been developed in the "Laboratoire d'Optique Atmosphérique," Lille, France, for measuring the BRDF (Bidirectional Reflectance Distribution Function) and the BPDF (Bidirectional Polarization Distribution Function) of surfaces in the field. It is equipped with 4 optical barrels, each of them carrying a different spectral filter. During the HAPEX-Sahel campaign, the 4 channels were centred at 450, 650, 850 and 1650 nm with passbands of 100 nm for the 1650 nm band, and 40 nm for the others. Polarizers rotate in front of the 4 detectors (3 photodiodes and one germanium for the longer wavelength band) and allow three successive measurements, C_1, C_2 and C_3, with three polarizer turned by steps of 45°.

The radiometer was mounted on a step-by-step electric engine which allows an inclination up to 75° on each sides of nadir viewing. An inclinometer provided automatically the zenith viewing angle of the radiometer and this information was stored with the measurements. The total angular sampling time from −75° to +75° was of 120 s. The apparatus (engine and radiometer) was mounted at the extremity of a 1.5 m length boom, at the top of a 7 m high mast. The field of view (FOV) was approximately 16° (total) which yields a footprint of 2 m diameter at nadir, so the boom allowed minimal contamination by the supporting mechanism. The mast was never in the instrument field of view, and its interception area was small which induced little shadowing or parasite light.

By rotating from +75° to −75°, the radiometer sampled the angular signature of the radiance in a vertical plane defined by its azimuth angle relative to the Sun. The azimuth angle could be changed easily by hand. The measurements were stored automatically on a micro-computer and a screen display provided a mean of checking the measurements. The angular signature of the reflectance is derived from measurements acquired with a varying surface cover as the radiometer rotates. Thus, a uniform surface is necessary to derive meaningful signatures.

B. Data Processing

The digital counts were converted to radiance using calibration coefficients. The calibration has been performed before and after the campaign in the laboratory, as well as on site with a calibrated reflectance panel. The calibrations gave coherent results within the method uncertainty which is of the order of ±5%. The radiances are then normalized to the top of the atmosphere (TOA) solar irradiance. The results are pseudo-reflectances since they do not account for the incoming

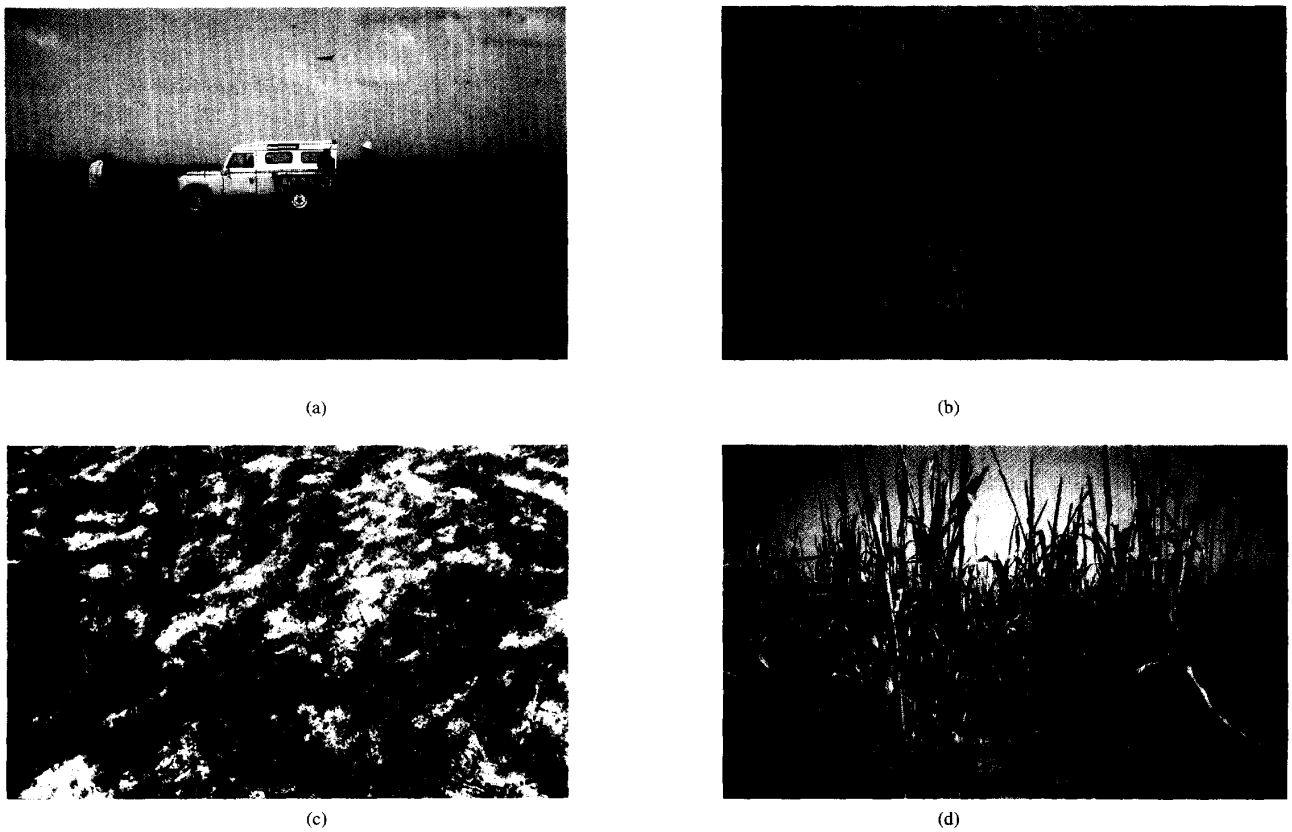

(a) (b) (c) (d)

Fig. 1. Ground oblique views for the four surfaces: (a) Site 1: Bare soil composed of sand and clay. (b) Site 2: Bare soil composed of clay with mid-size stones. (c) Site 3: Low and dense vegetation (*Zonnia glochidiatras* species). (d) Site 4: Millet.

radiance reduction on the downwelling path in the atmosphere. The surface reflectances are then under-estimated, all the more for the shorter wavelengths for which the atmospheric optical thickness is larger. One may argue that it would be better to normalize our mesurements to the incoming irradiance at the surface. However, as it is shown in Section V-C, the diffuse portion of the downwelling irradiance generates negligible polarization after reflection at the surface. Therefore, the downwelling irradiance is not an appropriate normalization quantity.

From these three calibrated measurements (ρ_1, ρ_2, ρ_3), one deduces the total reflectance ρ, the linear-polarized reflectance ρ_p and the polarization direction χ:

$$\rho = \frac{\rho_1 + \rho_3}{2} \tag{2a}$$

$$\rho_P = \frac{1}{\sqrt{2}}\left[(\rho_1 - \rho_2)^2 + (\rho_2 - \rho_3)^2\right]^{1/2} \tag{2b}$$

$$\sin(2\chi) = \frac{\rho_3 - \rho_1}{\rho_p}. \tag{2c}$$

As the polarized reflectance and the direction are obtained from a non-linear combination of larger terms ρ_1, ρ_2, and ρ_3 (2b) and (2c), they are then very sensitive to the noise on the ρ_i. It is expected that measurements over reflecting surface with small degree of polarization (i.e., ρ_p small relative to the individual ρ_i), like the vegetation in the infrared spectral domain, will have a relatively small signal to noise ratio that makes their analysis difficult.

C. The Sites

Four different surface covers have been investigated:

- A bare soil composed of sand and clay [site 1, Fig. 1(a)];
- A bare soil composed of clay with mid-size stones scattered on it [site 2, Fig. 1(b)];
- A low and dense vegetation, *zonnia glochidiatra* species [site 3, Fig. 1(c)];
- A field of millet [site 4, Fig. 1(d)].

The four sites have been investigated several times during the campaign from the end of August to the first days of October. Because of cloud coverage, only 15 days allowed useful measurements. During clear days, up to 35 angular scans from $-75°$ to $+75°$ have been acquired for varying solar zenith angles and relative azimuths.

These surface types are typical of the Sahel area. As already mentioned, our measurement procedure needs an uniform surface over several meters and so we did not investigate other dominant biomes such as the tiger bush or fallow. Although the measuring sites were chosen for their homogeneity, some irregularities in the angular signatures may be explained by the surface inhomogeneity.

IV. Models

A. Fresnel Equations

The models described hereafter assume that polarized reflectance from the surface is generated by single specular reflection, which is controlled by Fresnel equations. Fresnel reflection depends on the relative values of the two medium refractive indexes, as well as the incidence angle of the light on the interface. In what follows, we will recall this angle as the angle of reflection, γ.

A direction ω_x will be defined by its zenith angle, θ_x, and azimuth angle, ϕ_x. Hereafter, the index "s" stands for the Sun (or incident) direction, the index "v" for the instrument (or reflected) direction, and the index "n" for the normal to the individual reflector. The origin of the azimuth is the Sun direction ($\phi_s = 0$). The angle of reflection, γ, is the angle between the incident direction, ω_s, and the normal to the individual reflector ω_n. Note that γ is equal to half the phase angle. The following relations apply:

$$\gamma = 0.5 \cos^{-1} [\cos\theta_s \cos\theta_v + \sin\theta_s \sin\theta_v \cos\phi_v] \quad (3)$$

$$\theta_n = \cos^{-1} \left[\frac{\cos\theta_s + \cos\theta_v}{2\cos\gamma} \right]. \quad (4)$$

We also define the polarized Fresnel reflection coefficient:

$$F_P(\gamma) = \frac{1}{2}(r_\perp^2 - r_=^2) \quad (5)$$

where $r_\perp$ and $r_=$ are respectively the perpendicular and parallel Fresnel reflection coefficients given by

$$r_\perp(\gamma) = \frac{N\mu_T - \mu_I}{N\mu_T + \mu_I} \text{ and } r_=(\gamma) = \frac{N\mu_I - \mu_T}{N\mu_I + \mu_T} \quad (6a)$$

$$\mu_I = \cos\gamma \text{ and } \mu_T = \left[1 - \frac{\sin^2\gamma}{N^2} \right]^{1/2} \quad (6b)$$

where N is the refractive index of the reflective medium (the index of air is approximated to 1).

B. Vegetation Model

Previous measurements of the polarized reflectance of vegetation have shown that it is principally generated by specular reflectance on the leaf surface. Thus, the polarized reflectance is controlled by 1) the Fresnel reflectance (i.e. the reflection angle and the refractive index); 2) the leaf orientation distribution; and 3) the attenuation of the radiance on the incident and outgoing paths within the canopy.

From these considerations, several authors have derived theoretical models for the polarized reflectance of vegetation canopies [33], [41], [43]. Following [33], if the leaf inclination distribution is uniform, the polarized reflectance ρ_P can be simply written

$$\rho_P(\theta_s, \theta_v, \varphi) = \frac{F_P(\gamma)}{4(\cos(\theta_s) + \cos(\theta_v))} \quad (7)$$

where F_P is the polarized fraction of the specular reflectance as given by Fresnel law in (5). The model should be valid for many vegetation canopies with a complete ground cover (i.e., large leaf area indexes).

C. Bare Soil Model

The model for the polarized reflectance for a bare surface is different than that for a vegetation canopy. The model supposes that the polarized reflectance is generated by the soil surface. Thus, contrarily to the model for the vegetation, it does not consider any attenuation on the incident and outgoing path. This does not imply that no light is transmited through the soil, but we assume that the polarized light generated by this process is negligible. The model assumes that the ground is composed of isotropically distributed facets (rough surface). One representation for such a distribution is obtained considering the surface to be entirely covered with hemispheres of varying radii. Note that the ratio of the total surface of the spheres to the *macroscopic* horizontal surface is 2. Each facet is a specular reflector and the shading is neglected. The model is then similar to the case studied for a water surface [1], except for the slope angular distributions.

We consider an horizontal surface S, the size of which is much larger than the roughness length scale. Over this area, many individual facets have their normal oriented upward within $d\omega_n$. The integrated surface of these facets is

$$dS = S\frac{d\omega_n}{\pi}. \quad (8)$$

These facets spectrally reflect a polarized flux $dE^{\Uparrow}(\omega_v)$ into direction ω_v

$$dE^{\Uparrow} = E^{\Downarrow} \cos\gamma F_P(\gamma) dS \quad (9)$$

where the fluxes $E^{\Downarrow}$ and $dE^{\Uparrow}$ are measured perpendicular to the incident and reflected rays, respectively. We assume a monodirectional incident light. Simple trigonometry (when referring the normal and view directions to the incident direction, see Appendix A for detail) shows that

$$d\omega_v = 4\cos\gamma \; d\omega_n \quad (10)$$

$$dE^{\Uparrow} = \frac{E^{\Downarrow} F_P(\gamma) S \; d\omega_v}{4\pi} \quad (11)$$

and the reflected polarized radiance is

$$L^{\Uparrow}(\omega_v) = \frac{E^{\Downarrow} F_P(\gamma)}{4\pi \cos(\theta_v)}. \quad (12)$$

Using the definition of a reflectance, we obtain the polarized reflectance for a bare surface

$$\rho_P(\theta_s, \theta_v, \varphi_v) = \frac{F_P(\gamma)}{4\cos\theta_s \; \cos\theta_v}. \quad (13)$$

This formulation is clearly not satisfying for limb viewing or illumination as it leads to infinite values for those angles. This results from our approximation of neglecting mutual shadowing of the facets. However, it should give coherent results for smaller zenith angles.

V. Results

As it has been already emphasized by [8], atmospheric conditions may affect the measurements of surface reflectance even at surface level, so we give in Section V-A the turbidity conditions. Unless differently stated, the polarized reflectance

TABLE I
SUMMARY OF THE SUBSET OF MEASUREMENTS USED IN THIS PAPER, TOGETHER WITH THE MEASURED AEROSOL OPTICAL THICKNESS AT 450 nm

	Aug. 31	Sep. 01	Sep. 03	Sep. 05	Sep. 06	Sep. 09	Sep. 17	Sep. 22	Sep. 25	Sep. 26	Sep. 28	Sep. 29	Oct. 06	Oct. 07	Oct. 08
Optical Thickness	-	0.40	0.25	0.4	0.40	0.5	0.4	0.5	0.7	0.85	0.85	1.15	0.40	0.35	0.35
Site 1 Bare Soil 1	X	X									X	X			
Site 2 Bare Soil 2			X												
Site 3 Grass				X	X				X	X					
Site 4 Millet						X	X	X					X	X	X

measured over bare soils will be that acquired at 1650 nm, we make this choice since atmospheric effects are the smallest at this wavelength. For measurements over the vegetation, we will use the 650 nm data because those collected in the infrared are too noisy, due to the large total reflectance at these wavelengths (see Section III-B). Polarized reflectances as a function of the view angle are given in Section V-B when the spectral dependence is analyzed in Section V-C. In Section V-D, we analyze the polarization direction, and in Section V-E the particular case of the backscattering direction.

A. Turbidity Conditions

For the 15 days during which we acquired measurements, we indicate in table 1 the surface cover that was investigated, as well as the aerosol optical thickness at 450 nm (τ_{450}). As it can be seen in table 1, many measurements were acquired in relatively clear conditions $0.25 \leq \tau_{450} \leq 0.4$. Such turbidity values are very frequent in Sahelian regions. Several turbid days are also available, which allow an illustration of the atmospheric scattering effect on the measurements (26/09, 28/09, and 29/09).

B. Polarized Reflectance

Figs. 2–4 show typical angular signatures of the polarized reflectance in the principal plane. We recall that the reflectances are positive (respectively negative) when the polarization is perpendicular (respectively parallel) to the plane of scattering. On each diagram, the solid line shows the model results and the diamonds indicate the measurements. We use one of the two models defined in (7) and (13) according to the underlying surface.

Both models account for single specular reflection only. Thus, their estimates are always positive and vanish in the antispecular direction. The models fail to reproduce the negative polarization often observed close to backscattering. We discuss this particular feature in V–E The negative branch of polarized reflectance does not exceed −0.5% (dimensionless) over bare soil and −0.2% over vegetation.

Measurements plotted in Fig. 2(a) have been acquired over bare soil (site 1) on Sept. 1, with a large solar zenith angle of 65°. The polarized reflectance is negative close to the antispecular direction and increases up to 14% for a viewing

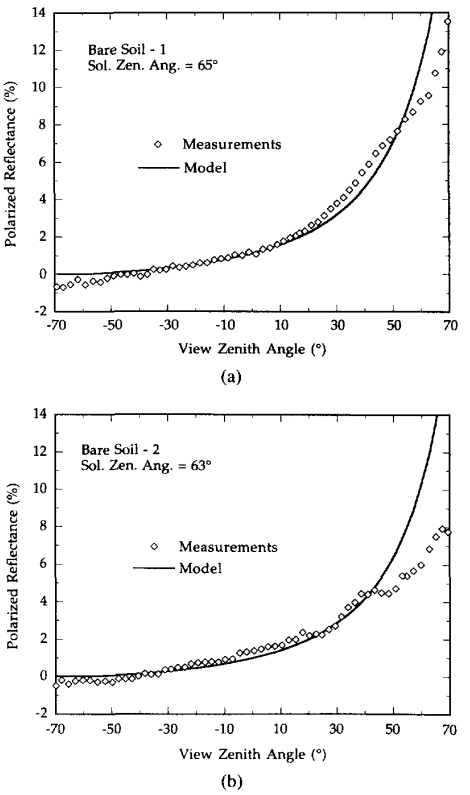

Fig. 2. Polarized reflectance measured in the principal plane at $\lambda = 1650$ nm as a function of the view angle. The full line results from model computation (see Section IV). The backscattering direction is on the left side of the plots. In (a) and (b) the underlying surface is site 1 and 2 respectively.

angle of 70° (the angle of reflection is then 67.5°). The model accurately reproduces the measurements away from the backscattering direction assuming a refractive index of 1.50. It slightly underestimates the observations for view angles between 30° and 50° and overestimates the measurements for view angles greater than 50°. Fig. 2(b) displays similar results for the second site of bare soil sampled on Sept. 3. The model is very accurate for view angle up to 45°. For larger view angles, it clearly overestimates the observations.

We find that the largest polarized reflectances are larger for site 1 (14%) than for site 2 (8%). One explanation for this feature is the difference in the texture of the two sites. Site 2 shows a number of stones whose influence on the reflectance for large angles may be large (shadowing). Another possible explanation results from the occurrence of rain the day before the measurements were acquired. Some spots within the site may have a large soil moisture content which tends to lower the refractive index and thus the specular reflectance [19]. The texture may also have been modified by the rain [3] but these are only hypothesis.

Fig. 3 is for the low and dense vegetation site acquired on Sept. 6. The measurements are here compared with the model designed for the vegetation, the refractive index of epicutilar wax, $m = 1.50$, was assumed [40]. This model predicts smaller

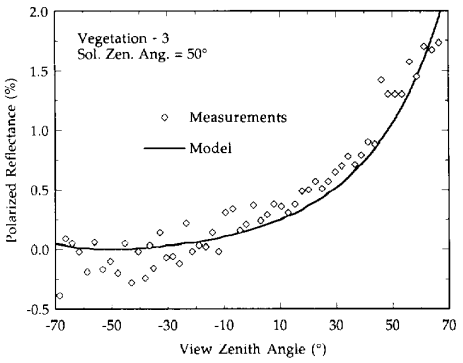

Fig. 3. Same as in Fig. 2 but for site 3 at $\lambda = 650$ nm.

polarized reflectances (around 2%) than for the bare soil and it is confirmed by the measurements. The angular signature is well reproduced, although the measurements are noisier.

The measurements over millet (site 4) are even smaller. In Fig. 4(a), they do not exceed 0.5%. Other measurements acquired over this site show larger polarized reflectance for sun angles closer to the zenith, but they never exceed 1%. The model clearly fails for this vegetation canopy, although it still gives satisfactory results for smaller zenith angles. One explanation for the millet particular behavior is the presence of "heads" at the top of the canopy that may be poor specular reflectors as discussed in [33] for corn and in [18] for wheat canopy. The heads shade the lower layer leaves and may therefore decrease the polarized reflectance. This hypothesis is confirmed by additional measurements acquired with similar conditions but for a smaller solar zenith angle of 31° on Oct. 8 [Fig. 4(b)]. This figure shows that, when the Sun is higher, the model performs better for off-nadir observations until 50° instead of 20°. When the Sun is higher, the interception by the heads (which are oriented in the vertical direction) is smaller and the model gives a better description of the radiative transfer in the canopy. The polarized reflectance angular signature of the millet is different from that measured for other vegetation coverage or bare soil and we cannot, therefore, conclude that it is a result of an atmospheric effect. Our data and the comparison with the model provides further evidence that the "heading" of a canopy decreases the polarized reflectance and may therefore be detected with such measurements.

Figs. 5–7 display similar results corresponding to the same 4 sites albeit in the perpendicular plane. For this geometry, the range of phase angle covered when varying the view angle is more limited than in the principal plane: For a solar zenith angle of 60° and a view angle that varies between −60° and 60°, the angle of reflection varies between 30° (at nadir viewing) and 38° (at ±60° view angle). Similar conditions in the principal plane were induced angles or reflection that vary between 0° (backscattering) and 60° (forward scattering). The variations in polarized reflectance are then much smaller in the perpendicular plane than in the principal plane as predicted by the models because of the restricted range of angles or reflection.

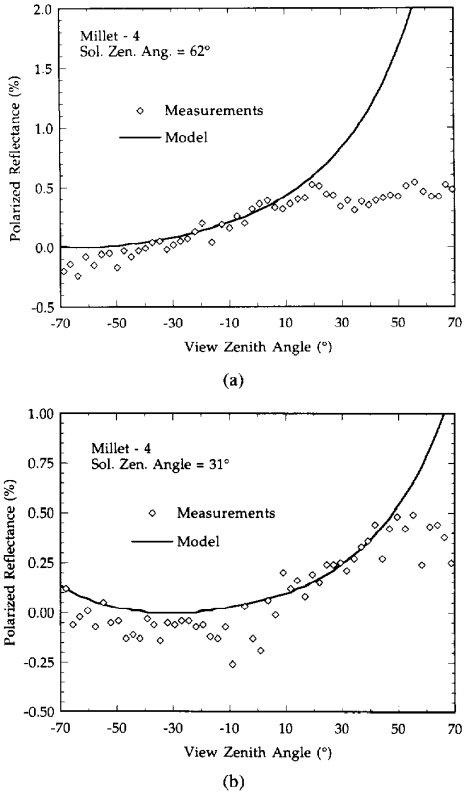

Fig. 4. Same as in Fig. 2 but for site 4 at $\lambda = 650$ nm. (a) A solar zenith angle of 62°, (b) A solar zenith angle of 31°.

The measurements should be symmetric to the nadir direction. Although the general signature is indeed symmetric, there are some departures from symmetry that result from surface heterogeneities. For grazing observations, the models fail for similar reasons as that in the principal plane, and they give larger results than the measurements. The approximations we made on the mutual shading of the reflecting elements fail for these geometries. However, the models allow a fairly accurate representation of the order of magnitude of the polarized reflectance for view angles up to $\approx 50°$.

C. Spectral Signature of the Polarized Reflectance

Following the hypothesis that the polarized light mostly results from specular reflection on the leaf surface or on bare ground facets, it should be spectrally neutral provided that the refractive index is constant over the spectral interval considered. Fig. 8(a) and (b) show polarized reflectances measured for several viewing directions in the 3 shortest wavelengths as a function of polarized reflectances measured at 1650 nm, Fig. 8(a) is for measurements over a bare ground collected on Sept. 03 and Fig. 8(b) for measurements over vegetation on Sept. 26. A large correlation between the various wavelengths is obtained for bare soil. Correlation is also observed for vegetation but with a larger dispersion. In Fig. 8(a), there is a constant ratio of about 0.5 between the polarized reflectance at 450 nm and that at 1650 nm. For other measurement sets,

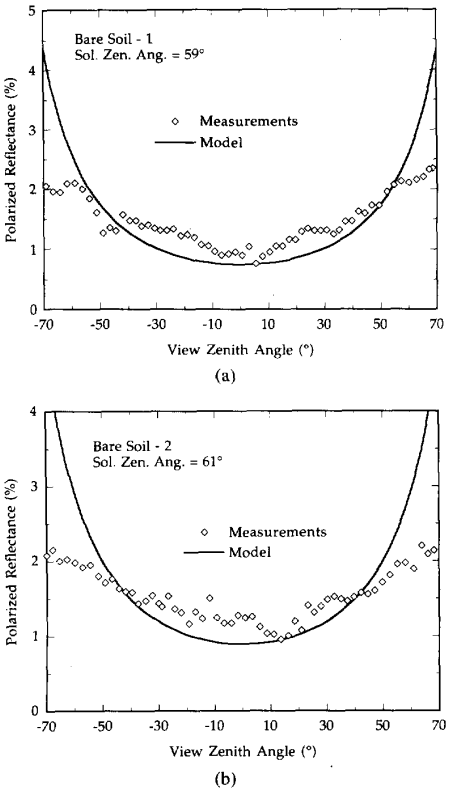

Fig. 5. Same as in Fig. 2 but in the perpendicular plane.

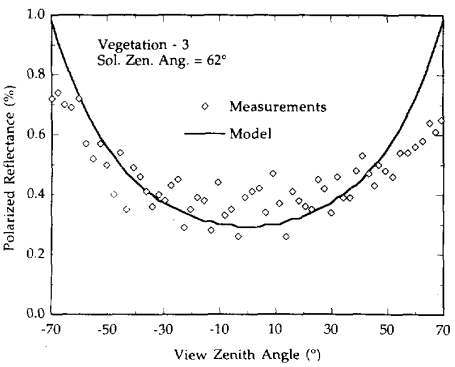

Fig. 6. Same as in Fig. 3 but in the perpendicular plane.

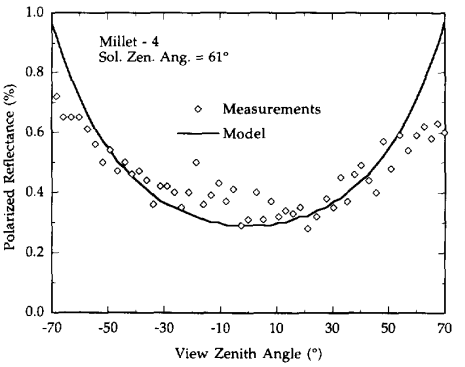

Fig. 7. Same as in Fig. 4 but in the perpendicular plane.

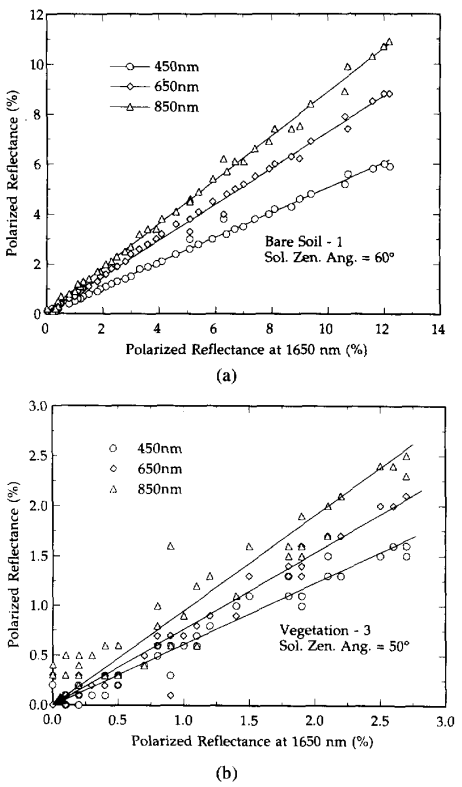

Fig. 8. Polarized reflectances measured in the principal plane for several wavelengths. The measurements at 450 nm (circles), 650 nm (diamonds), and 850 nm (triangles) are shown as a function of that at 1650 nm. (a) The underlying surface is bare soil and the solar zenith angle is 60°. (b) The underlying surface is low vegetation and the solar zenith angle is 50°.

this ratio varies between 0.36 and 0.67. Two optical effects may explain this difference:

The Fresnel polarized reflectance depends on the refractive index, which may be wavelength dependent. Fig. 9 plots the Fresnel polarized reflectance, as defined in Section IV-A, as a function of the angle of reflection. It shows a large dependence on the refractive index. The ratio of 2 observed in Fig. 8(a) could be explained if, for instance, the refractive index was 1.30 at 450 nm and 1.60 at 1650 nm. From the few data published in the literature, such a variation is very questionable. Terrestrial materials have generally smaller refractive indexes in the near infrared than in the visible or at the most constant [30], [38]. A similar conclusion is expected for vegetation [40].

The second possible explanation of the spectral variations of the polarized reflectance is related to atmospheric effects. Atmospheric scattering reduces the amount of solar light that reaches the surface. Moreover, the light scattered in the atmosphere but which still reaches the surface has a diffuse

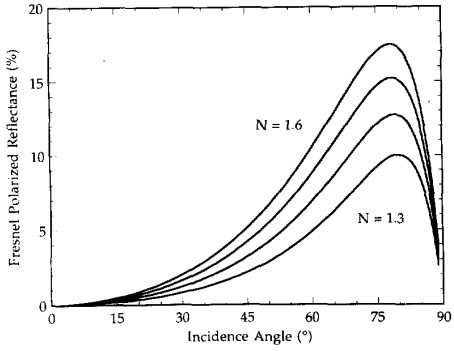

Fig. 9. Polarized fresnel reflection coefficient, as defined in (5), as a function of the incidence angle. The refractive index increases from 1.3 (lower curve) to 1.6 (upper curve) by step of 0.1.

angular distribution and may not generate polarized light as does the direct solar beam. A larger atmospheric optical thickness yields, therefore, a smaller apparent polarized reflectance. Several observations support this second hypothesis. First, we see that the spectral variations of the polarized reflectance (Fig. 8) are coherent with this hypothesis and the fact that the optical thickness decreases with increasing wavelength. We note that the ratio departure from unity increases with the solar zenith angle, which is coherent with an increase in optical path with the air mass. Fig. 10(a) illustrates this finding for the ratio of measurements acquired at 450 nm and 1650 nm over bare soil on Sept. 3. Similarly, Fig. 10(b) is for the wavelengths 450 nm and 650 nm acquired over vegetation on Sept. 26. These data were chosen for the stability of the atmospheric optical thickness over the day.

We computed for each dataset the best linear fit between the various wavelength polarized reflectance (such as those of Fig. 8). We then plotted the resulting slope as a function of the optical air mass ($1/\cos\theta_s$) for all sequences acquired during a given day (and thus for varying solar angles). If our hypothesis is correct, the ratio of the two wavelength polarized reflectances (and thus the best fit slope) should be equal to

$$R(\lambda_1, \lambda_2, \mu_s) = \exp\left(-\frac{\tau_1 - \tau_2}{\cos(\theta_s)}\right) \tag{14}$$

where τ_1 and τ_2 are related to the atmospheric optical thickness for the two wavelengths. If the direct solar beam was the only source of polarized reflectance, τ_1 and τ_2 should be equal to the optical thicknesses. However, because of the forward peak of the phase function, a large fraction of the radiance scattered by aerosols has a direction close to the direct solar beam, and may then participate to the polarized reflectance as unscattered radiance does. Thus τ_1 and τ_2 may be *smaller* than the total atmospheric optical thicknesses. On the other hand, since radiance scattered by molecules shows an almost isotropic angular distribution, we expect τ_1 and τ_2 to be *larger* than the molecular optical thickness. Similarly, $(\tau_2 - \tau_1)$, which is positive assuming that $\lambda_1 > \lambda_2$, is expected to be larger than the molecular optical thickness difference, but smaller than the total optical thickness difference.

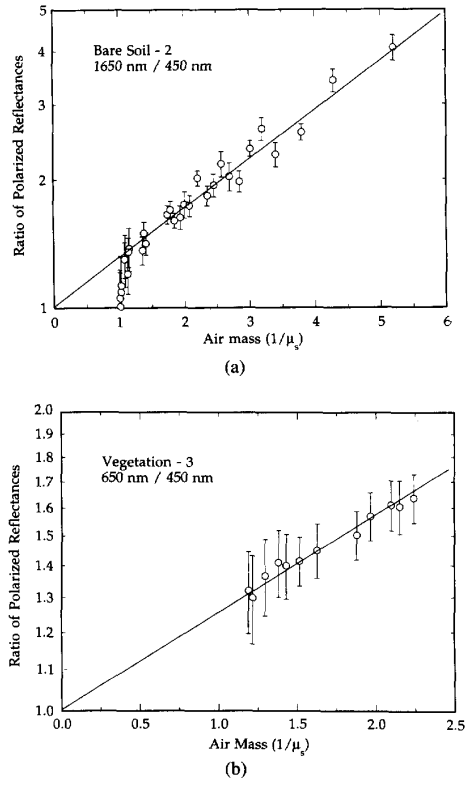

Fig. 10. Spectral variation of the polarized reflectances as a function of the optical air mass. The spectral variation is derived from the slope of a linear fit over data sets such as those of Fig. 8 (a slope of 1 corresponds to no spectral variation). Each dot corresponds to one data set and all data sets acquired during a given day are represented on the figure. The error bars arer elated to the scatter around the best fit. (a) Measurements over bare ground on Sept. 3 for 1650 nm and 450 nm. (b) Measurements over vegetation on Sept. 26 for 650 nm and 450 nm.

In Fig. 10(a), we find $(\tau_2 - \tau_1)$ =0.27 which is, as expected, larger than the molecular optical thickness difference (0.22) but smaller than the total optical thickness difference (0.37). In Fig. 10(b), we find $(\tau_2 - \tau_1) = 0.23$ whereas 0.17 is expected for a pure molecular atmosphere and the measurement gave a total optical thickness difference of 0.24.

Fig. 10(a) and (b) demonstrate that the constant ratio found in the polarized reflectance measurements at various wavelengths is correlated with the Sun angle. The variations found are coherent with the hypothesis that photons scattered in the atmosphere participate little to the polarized radiance after reflection at the surface. We conclude that the constant ratios between the various wavelength measurements result mostly from the spectral transmittance of the atmosphere on the downward path.

We performed a second validation of our assumption. We selected measurements acquired over bare soil with a very large optical thickness on Sept. 28 and 29 (Table I) with a Sun angle of 55° for both days. We then plotted the polarized reflectance at 450 nm as a function of measurements at 1650 nm (Fig. 11). As expected, the measurements are well correlated and much smaller at 450 nm than at 1650 nm. As

the optical properties of the atmosphere were measured, we can correct the polarized reflectance for transmission effects at the two wavelengths. As a first step, we simply divide the measurements by the direct transmission expressed by

$$T_\lambda = \exp\left(-\frac{\tau_{a\lambda} + \tau_{m\lambda}}{\cos(\theta_s)}\right) \tag{15}$$

where $\tau_{a\lambda}$ and $\tau_{m\lambda}$ are the aerosol and molecular optical thickness, respectively, at the corresponding wavelength. Polarized reflectances are overcorrected since the polarized reflectances are then larger at 450 nm than at 1650 nm (Fig. 11, correction a). Assuming that 30% of the diffuse light is still directional [37], which means that only 70% of the aerosol optical thickness has to be corrected for, the polarized reflectances at the two wavelengths are quite similar (Fig. 11, correction b). Note that some uncertainty results from the hypothesis that the aerosol phase function (and therefore the percentage of scattered light in the forward peak) does not change with wavelength. We demonstrate that the constant ratio found in the polarized reflectance measurements at various wavelengths results from atmospheric scattering and absorption. The spectral variations support the hypothesis that the radiance scattered at large angles does not contribute significantly to the reflected polarized reflectance.

The results from this section suggest that our measurements should be corrected for atmospheric transmitssion as in (15), with a reduced aerosol optical thickness. We have *not* corrected our measurements for atmospheric transmission because of the uncertainty in the aerosol optical thickness to be used. On the other hand, relatively clear days were selected for model-measurement comparisons whereas more hazy days have been used to demonstrate the atmospheric effect on the reflectance spectral signature. Moreover, for model-measurement comparisons, we selected the longer usable wavelength as the atmospheric optical thickness decreases with increasing wavelength. Although limited (on the order of 25% depending on the day and the solar angle) the correction would increase the surface polarized reflectance, and the agreement with the model would be reduced.

D. Polarization Direction

The polarization direction is derived from the three polarized measurements with the polarizers turned by steps of 45° (2c). As for the polarized reflectance, it may be noisy when the degree of polarization is small. In the perpendicular plane, we find the polarization direction always perpendicular to the plane of scattering (within the measurement accuracy). It confirms that single specular reflection processes control the polarized reflectance.

Similarly, in the principal plane, away from the backscattering direction, the polarization direction is found perpendicular to the plane of scattering ($\chi = 90°$) as shown in Fig. 12(a) and (b). Close to the backscattering direction, however, polarization resulting from single specular reflection vanishes because the polarized Fresnel reflection coefficient does so (see Fig. 9). Thus, in those directions, we observe the polarization generated by other processes. We will now analyse in more detail the measurements in this geometry of observation.

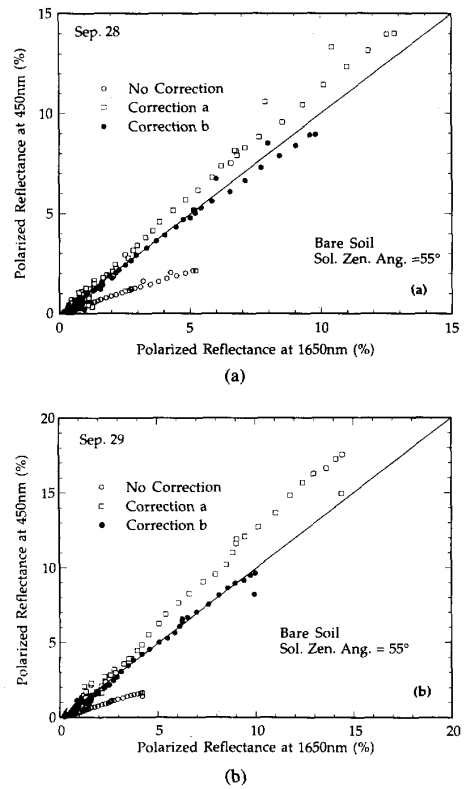

Fig. 11. Polarized reflectances at 450 nm as a function of polarized reflectances at 1650 nm. The open circles correspond to the raw data (no correction), the squares to data which have been corrected for the transmission function computed with the total aerosol optical thickness (correction a), the full circles to data which have been corrected for the transmission function considering that 30% of the diffuse flux is still directional (correction b). (a) Data collected on Sept. 28, (b) Data collected on Sept. 29.

E. The Backscattering Direction

Fig. 12(a) and (b) plot the polarized direction estimated over bare soils and vegetation in the principal plane at 450 nm and 1650 nm. Close to backscattering, there is an obvious difference between the two wavelengths. At 1650 nm, negative polarization are observed in backscattering directions for both surfaces even if the noise is larger for vegetation as expected. Reference [44] showed that geometric considerations on the possible ray paths on a rough surface explain the negative polarization measured in the backscattering direction when observing distant planets or bare ground samples: "Negative polarization is found to be caused by shade and shadows affecting the double-reflected rays." Similar considerations as for the bare soil can be also developed over vegetation [Fig. 12(b)]. Reference [43] showed that the light transmitted through a leave is negatively polarized and may therefore have an effect on the polarization direction. We note however that the amount of transmitted light is very small and that it requires another scattering/reflectance process to affect the polarization in the antispecular direction. We therefore have to consider multiple surface reflections, which our models do not consider, for interpreting the negative values at 1650 nm.

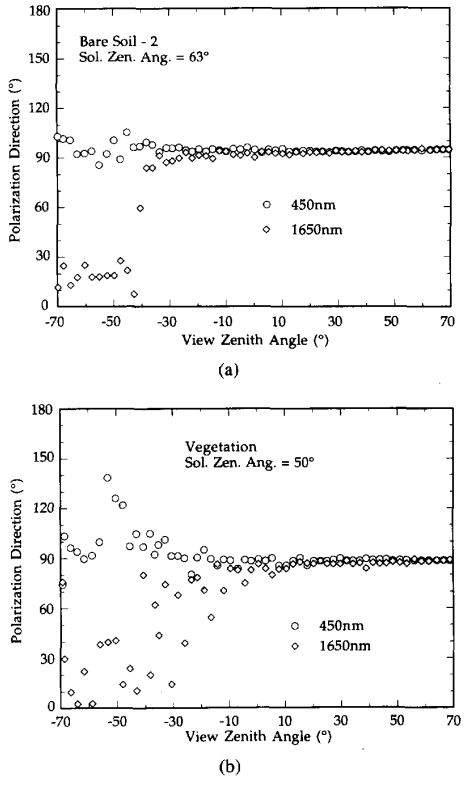

Fig. 12. Polarization direction estimated at 450 nm (circles) and at 1650 nm (diamonds) as a function of the view angle. The directions are estimated with respect to the scattering plane. (a), The underlying surface is bare soil (site 1) and the solar zenith angle is 63°. (b) The underlying surface is dense vegetation (site 3) and the solar zenith angle is 50°.

The interpretation developed in [44] for the negative polarization in the backscattering direction implies a spectrally neutral polarized reflectance. Our observation shows a large spectral variation since we actually find a *positive* polarization at 450 nm. Thus, another process generating polarized light is necessary to explain our observation in the backscattering direction.

Since atmospheric scattering is wavelength dependent and is a generator of polarized light, it is an obvious candidate. We therefore try to modelize the interaction of atmospheric scattering and surface reflection. In Appendix B, we develop a semi-analytical model for the evaluation of the polarized reflectance resulting from photons scattered by atmospheric molecules and then reflected spectrally by the surface. For solar angles less than 70°, the model predicts a polarized reflectance perpendicular to the plane of scattering (positive polarization). Since this process is much larger for the shorter wavelengths, the sign of the polarization is right for explaining the removal of negative polarization at 450 nm. However, the predicted magnitude is too small since the resulting polarized reflectance is smaller than 0.04% (Fig. 13). Because the various contributions to the polarized reflectance have their plane of scattering oriented variously, they tend to cancel one another and result in almost unpolarized light.

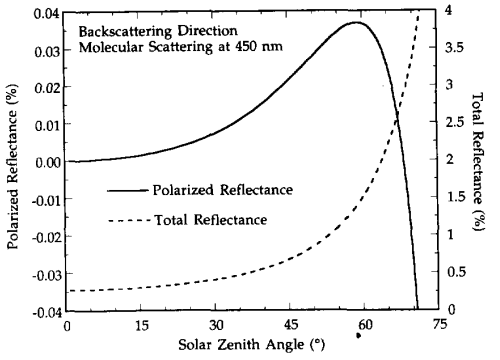

Fig. 13. Estimate of the total (right axis) and *polarized* (left axis) reflectances resulting from single scattering in the atmosphere and specular reflection at the surface. The estimate is made for a molecular atmosphere of optical thickness 0.22 and for varying solar zenith angle. The direction of observation is the backscattering (or anti-solar).

Aerosol may also have an effect on the polarized reflectance in the backscattering direction, although we have not been able to evaluate it since we lack the necessary information on their polarized phase function. We found that the observed spectral variation varies with the view angle, which favors this hypothesis.

Another process which we did not consider so far and that may influence the polarized reflectance in the backscattering direction is the interaction of specular and diffuse reflection at the surface: The negative polarization would result from specular reflection of the light already scattered by non specular processes (those that generate unpolarized reflectance). In the backscattering direction, we found some correlation between the polarized reflectance and the total reflectance, which favors this hypothesis. At 450 nm, since the surface reflectance is small, the polarization generated by the process described above is negligible. On the other hand, atmospheric scattering, which is the largest at this wavelength, can explain the positive polarization measured in the backscattering direction.

VI. Summary and Discussion

In this paper, we have investigated the polarized reflectance from natural surfaces. We have analyzed the measurements acquired over bare soils, a dense canopy, and a field of millet, and we compared these observations to the predictions of two analytical models. One model is designed for bare soils and the other for vegetation canopies. They both assume that the polarized reflectance is generated by single specular reflection over isotropicaly distributed facets (bare soil) or leaves (vegetation). The two physically based models need only one variable parameter; the refractive index of the reflecting medium.

The spectral variations of the polarized reflectance, which seem contradictory with our hypothesis that polarized reflectance is generated by specular reflection, can be explained by atmospheric scattering on the downwelling path. Molecular scattering generates diffuse light that contributes very little to

the polarized reflectance after reflection at the surface. On the other hand, some part (on the order of 30%) of light scattered by aerosols is slightly modified and contributes to the polarized reflectance as the direct solar beam does. This result shows that the polarized reflectance measurements need to be corrected for atmospheric transmission, depending on the wavelength and the aerosol optical thickness. Because the exact magnitude of the correction is unknown, we decided to present our measurements normalized to the top of the atmosphere irradiance. In order to reduce the uncertainty, we selected the relatively clear days in our dataset, and we used the longer usable wavelength (the atmospheric optical thickness is then smaller).

Besides the uncertainty discussed above, we found a large agreement between the model predictions and the measurements, collected in the field over various surface coverages and solar angles. In particular, the observations confirm that, for similar geometries, the polarized reflectance generated by the bare soil is much larger than that generated by the vegetation. The largest polarized reflectances observed over bare soils are on the order of 12%, whereas they never exceed 3% over the vegetation. The models accurately estimate the polarized reflectance angular signature for zenith angles up to about 55°. For larger zenith view angles, the approximations concerning the mutual shading of reflecting elements fail, and the observations are smaller than the model predictions.

In the backscattering direction, polarized reflectance generated by single specular reflection vanishes. The model predicts no polarized reflectance in that direction, whereas the observations show a small polarization which varies with the wavelength. We have not been able to identify precisely the origin of this polarization although several hypothesis were raised.

Our results suggest that dense vegetation covers will generate a constant polarized reflectance provided that their leaves have similar refractive indexes. This is not necessary true for vegetation with a large density of not-leaf-like elements. Therefore, "typical" vegetation cover cannot be discriminated from their polarization signature, although a particular event such as the "heading" of a canopy can be detected with this technique. However, we acknowledge that our results have been acquired over a limited set of surface covers and that further measurements are needed to confirm our statement.

In the context of spaceborne remote sensing, our results suggest that the information content of polarized reflectance is relatively poor for vegetation monitoring but can be very useful for aerosols remote sensing. To estimate aerosol optical thickness and characteristics from polarized reflectance measurements, one must first substract the surface signal and our models can be used to estimate the surface contribution with a limited knowledge of the surface cover characteristics. It is clear that if the aerosol polarized reflectance is smaller than the surface signal, the relative error will become large. Still, in that case, the models can indicate view directions that are the most appropriate for aerosol remote sensing (those for which the surface polarized reflectance is small). A forthcoming paper will present comparisons of airborne polarized measurements with surface observations described in this paper.

APPENDIX A

In this appendix, we show that, for a monodirectional incident light, the normal and view direction solid angle are related by the relation

$$d\omega_v = 4\cos\gamma\, d\omega_n. \tag{A1}$$

The demonstration refers the two directions not relative to the vertical but to the incident direction. We use α and ψ, respectively, as the zenith and azimuth directions relative to the incident direction. All other notations are unchanged. The following equations apply:

$$\alpha_v = 2\alpha_n = 2\gamma \tag{A2}$$

$$\psi_v = \psi_n. \tag{A3}$$

We can then write

$$\begin{aligned} d\omega_v &= \sin\alpha_v d\alpha_v d\psi_v \\ &= 4\cos\alpha_n \sin\alpha_n d\alpha_n \\ &= 4\cos\gamma d\omega_n \end{aligned} \tag{A4}$$

which proves (A1).

APPENDIX B

In this appendix, we evaluate the polarized reflectance in the backscattering direction that results from single scattering in the atmosphere, followed by specular reflection at the surface. We will assume a molecular atmosphere (no aerosols).

As in the main section of the paper, the index "s" is for the solar direction and the index "v" for the view direction. We add the index "i" (for incident) for the direction of the rays after scattering and before specular reflection. Since we are only interested in the backscattering direction, we have $\omega_s = \omega_v$.

We first evaluate the luminance at the surface after single scattering in the atmosphere. We distinguish the two components parallel and perpendicular to the plane of scattering

$$L^{\Downarrow}_{i=}(\omega_i) = E_0 \frac{e^{-\frac{\tau}{\mu_s}} - e^{-\frac{\tau}{\mu_i}}}{\mu_s - \mu_i} \frac{P_{m=}(\alpha)}{4\pi} \tag{B1a}$$

$$L^{\Downarrow}_{i\perp}(\omega_i) = E_0 \frac{e^{-\frac{\tau}{\mu_s}} - e^{-\frac{\tau}{\mu_i}}}{\mu_s - \mu_i} \frac{P_{m\perp}(\alpha)}{4\pi} \tag{B1b}$$

where E_0 is the solar flux at the top of the atmosphere, and $P_{m=}$ and $P_{m\perp}$ are the parallel and perpendicular components of the molecular phase function (we neglect the depolarization factor)

$$P_{m=}(\alpha) = \frac{3}{4}\cos^2(\alpha) \tag{B2a}$$

$$P_{m\perp}(\alpha) = \frac{3}{4} \tag{B2b}$$

and α is the scattering angle

$$\cos(\alpha) = \cos(\theta_s)\cos(\theta_i) + \sin(\theta_s)\sin(\theta_i)\cos(\phi_i). \tag{B3}$$

For the specular reflection at the surface, we make the same assumptions as for the bare soil specular reflection model developed in Section IV-B. The downwelling radiance $L^{\Downarrow}$ in solid angle $d\omega_i$ contributes to the upwelling radiance $dL^{\Uparrow}$ in direction ω_v

$$dL^{\Uparrow}_{=} = \frac{L^{\Downarrow}_{=}(\omega_i) r^2_{=}(\gamma)}{\cos(\theta_v)} \frac{d\omega_i}{4\pi} \tag{B4a}$$

$$dL^{\Uparrow}_{\perp} = \frac{L^{\Uparrow}_{\perp}(\omega_i) r^2_{\perp}(\gamma)}{\cos(\theta_v)} \frac{d\omega_i}{4\pi} \tag{B4b}$$

where γ is the incidence angle and $r(\gamma)$ are the Fresnel reflection coefficients defined in (4). Note that, because $\omega_s = \omega_v$, we have $\gamma = \alpha/2$.

The two components of the upwelling luminance can then be integrated over the incident direction ω_i. However, the plane of scattering changes with the incident direction. Thus, one shall first project the two components of the polarized reflectance into the vertical and horizontal planes

$$dL^{\Uparrow}_{b} = \cos^2(\chi) dL^{\Uparrow}_{=} + \sin^2(\chi) dL^{\Uparrow}_{\perp} \tag{B5a}$$

$$dL^{\Uparrow}_{\leftrightarrow} = \cos^2(\chi) dL^{\Uparrow}_{\perp} + \sin^2(\chi) dL^{\Uparrow}_{=} \tag{B5b}$$

where χ is the angle between the vertical plane and the plane of scattering

$$\cos(\chi) = \frac{\sin(\theta_s)\cos(\theta_i) - \sin(\theta_i)\cos(\theta_s)\cos(\phi_i)}{\sin(\alpha)}. \tag{B6}$$

The two components of the reflectance in the vertical and horizontal planes are then

$$R_b = \frac{\pi}{E_0} \int_{2\pi} dL_b \text{ and } R_{\leftrightarrow} = \frac{\pi}{E_0} \int_{2\pi} dL_{\leftrightarrow}. \tag{B7}$$

The total reflectance generated by the process described above is $R_{\leftrightarrow} + R_b$ and the polarized reflectance is $R_{\leftrightarrow} - R_b$.

Equations (B1) to (B7) allow one to compute the contribution to the polarized reflectance measured at the surface of the molecular single scattering followed by specular reflectance on isotropically distributed facets. The angular integration in (B7) cannot be solved analytically, but it is easily done numerically. Fig. 13 plots the results of the numerical integration for a molecular atmosphere at 450 nm ($\tau = 0.22$). The total reflectance is on the order of 0.27% for small solar zenith angles. It then increases regularly and is on the order of 1.5% for a solar zenith angle of 60°.

The polarized reflectance is much smaller. For solar zenith angle smaller than about 68°, the polarization is in the horizontal plane but it does not reach 0.04%. It then show a steep negative slope and is about −0.04% for a solar zenith angle of 70°.

The degree of polarization is smaller than 0.04 for solar zenith angles less than 75°. It shows that this reflectance process (scattering then specular) is a poor polarizer. Each individual contribution (the $dL^{\Uparrow}$) is strongly polarized since both successive processes (molecular scattering and specular reflection) polarize the light perpendicular to the plane of scattering. However, since the planes of scattering of all incident directions are variously oriented, these contributions to the polarized radiance tend to cancel one another. It is likely that higher order scattering/reflectance processes are little polarized for the same arguments.

ACKNOWLEDGMENT

The execution of a collaborative international experiment such as the HAPEX-Sahel experiment requires the dedicated efforts of a great many people, many of whom cannot be named here. The authors wish to thank their collaborators in Niger at DMN, DRE, University of Niamey, INRAN, Aéroport de Niamey Authority, Groupement Aérien National, AGRHYMET, ICRISAT and ACMAD.

The authors would like to specially thank J. Y. Balois, C. Devaux, A. P. Fattori, I. Jankowiak, C. Pietras, J. L. Roujean, and C. Verwaerde for helping them to set up the mast many (too many?) times during the field experiment.

REFERENCES

[1] F. M. Bréon, "An analytical model for the cloud free atmosphere/ocean system reflectance," *Remote Sensing Environ.*, vol. 43, pp. 179–192. 1993.
[2] F. M. Bréon and P. Y. Deschamps, "Optical and physical parameter retrieval from POLDER measurements over the ocean using an analytical model," *Remote Sensing Environ.*, vol. 43, pp. 193–209, 1993.
[3] J. E. Cipra, M. F. Baumgardner, E.R. Stoner, and R. B. MacDonald, "Measuring radiance characteristics of soil with a field spectroradiometer," *Soil Sci. Soc. Am. Proc.*, vol. 35, pp. 1014–1017, 1971.
[4] K. L. Coulson, E. L. Gray, and G. M. Bouricius, "A study of the reflection and polarization characteristics of selected natural and artificial surfaces," Tech. Informat. Series, Rep. R64SD74, General Electric Co., Missile and Space Div., Space Sciences Lab., 1964.
[5] P. J. Curran, "A photographic method for recording of polarized visible light for soil surface moisture indications," *Remote Sensing Env.*, vol. 7, pp. 305–322, 1978.
[6] ——, "The relationship between polarized visible light and vegetation amount," *Remote Sensing Environ.*, vol. 11, pp. 87–92, 1981.
[7] ——, "Polarized visible light as an aid to vegetation classification," *Remote Sensing Environ.*, vol. 12, pp. 491–499, 1982.
[8] D. W. Deering and T. Eck, "Atmospheric optical depth effects on anisotropy of plant canopy reflectances," *Int. J. Remote Sensing*, vol. 8, pp. 893–916, 1987.
[9] P. Y. Deschamps, F. M. Bréon, M. Leroy, A. Podaire, A. Bricaud, *et al.*, "The POLDER mission: Instrument characteristics and scientific objectives," *IEEE Trans. Geosci. Remote Sensing*, vol. 32, pp. 598–615, 1994.
[10] J. L. Deuzé, F. M. Bréon, J. L. Roujean, P. Y. Deschamps, C. Devaux *et al.* "Analysis of the POLDER (Polarization and directionality of earth's reflectances) airborne instrument observations over land surfaces," *Remote Sensing Env.*, vol. 45, pp. 137–154, 1993.
[11] A. Dollfus and D. L. Coffeen, "Polarization of Venus, I. Disk observations," *Astron. Astrophys.*, vol. 8, pp. 251–266, 1970.
[12] A. Dollfus, "Optical reflectance polarimetry of Saturn's globe and rings. I. Measurements on B ring," *Icarus*, vol. 37, pp. 404–419, 1979.
[13] W. G. Egan, "Aircraft polarimetric and photometric observations," *Proc. 5th Int. Symp. Remote Sensing Env.*, Ann Arbor, MI, pp. 169–189, 1968.
[14] ——, "Polarimetric and photometric simulation of the Martian surface," *Icarus*, vol. 10, pp. 223–227, 1969.
[15] ——, "Optical stokes parameters for farm crops identification," *Remote Sensing Env.*, vol. 1, pp. 165–180, 1970.
[16] B. W. Fitch, R. L. Walraven, and D. E. Bradley, "Polarization of light reflected from grain crops during the heading growth stage," *Remote Sensing Env.*, vol. 15, pp. 263–268, 1984.
[17] T. Gehrels, J. C. Gradie, M. L. Howes, and F. J. Urba, "Wavelength dependence of the polarization, XXIV. Observation of Venus," *Astron. J.*, vol. 84, pp. 671–682, 1979.

[18] R. Ghosh, V. N. Sridhar, H. Venkatesh, A. N. Mehta, and K. I. Patel, "Linear polarization measurements of a wheat canopy," *Int. J. Remote Sensing*, vol. 14, pp. 2501–2508, 1993.
[19] D. P. Gibbs, "Measurement and model comparisons of polarized bidirectional reflectances: A new approach to advance understanding of light interaction with natural scenes," Ph.D. dissertation, Univ. Texas, Arlington, 1992, p. 190.
[20] D. P. Gibbs, C. L. Betty, A. K. Fung, A. J. Blanchard, J. R. Irons, and W. L. Balsam, "Automated measurement of polarized bidirectional reflectance," *Remote Sensing Env.*, vol. 43, pp. 97–114, 1993.
[21] P. Goloub, M. Herman, J. L. Deuzé, and R. Frouin, "Optical properties of snow and ice derived from aircraft POLDER data," *Antarctic J. United States*, vol. 27, pp. 191–192, 1992.
[22] J. P. Goutorbe, T. Lebel, A. Tinga, P. Bessemoulin, J. Brouwer *et al.*, "HAPEX-SAHEL: A large scale study of land-surface interactions in the semi-arid tropics," *Ann. Geophysicae*, vol. 12, p. 53, 1994.
[23] L. Grant, "Diffuse and specular characteristics of leaf reflectance," *Remote Sensing Env.*, vol. 22, pp. 309–322, 1987.
[24] J. E. Hansen and J. W. Hovenier, "Interpretation of the polarization of Venus," *J. Atmos. Sci.*, vol. 31, pp. 1137–1160, 1974.
[25] J. E. Hansen and D. L. Travis, "Light scattering in planetary atmosphere," *Space Sci. Rev.*, vol. 16, pp. 527–539, 1974.
[26] M. Herman, J. Y. Balois, L. Gonzales, P. Lecomte, J. Lenoble *et al.*, "Stratospheric aerosol observations from a ballon-borne polarimetric experiment," *Appl. Opt.*, vol. 25, pp. 3573–3583, 1986.
[27] J. W. Hovenier, "Principles of symmetry for polarization studies of planets," *Astron. Astrophys.*, vol. 7, pp. 86–99, 1970.
[28] Y. Kawata, "Circular polarization of sunlight reflected by planetary atmospheres," *Icarus*, vol. 33, pp. 217–232, 1978.
[29] B. Lyot, "Recherches sur la polarization de la lumiére des planétes et de quelques substances terrestres," *Annales de l'Observatoire de Paris, Section de Meudon*, vol. VIII, no. 1, 1929.
[30] J. B. Pollack, O. B. Toon, and B. N. Khare, "Optical properties of some terrestrial rocks and glasses," *Icarus*, vol. 19, pp. 372–389, 1973.
[31] S. D. Prince, Y. Kerr, J. P. Goutorbe, T. Lebel, A. Tinga *et al.*, "Geographical, biological and remote sensing aspects of the hydrological and atmospheric pilot experiment in the Sahel (HAPEX-SAHEL)," *Remote Sensing Env.*, in press.
[32] G. Rondeaux and V. Vanderbilt, "Specularly modified vegetation indices to estimate photosynthetic activity," *Int. J. Remote Sensing*, vol. 14, pp. 1815–1823, 1993.
[33] G. Rondeaux and M. Herman, "Polarization of light reflected by crop canopies," *Remote Sensing Env.*, vol. 38, pp. 63–75, 1991.
[34] R. Santer and M. Herman, "Analysis of some Venus ground-based polarimetric observations," *Astron. J.*, vol. 84, pp. 1802–1810, 1979.
[35] R. Santer and A. Dollfus, "Optical reflectance polarimetry of Saturn's globe and rings, IV. Aerosols in the upper atmosphere of Saturn," *Icarus*, vol. 48, pp. 496–518, 1981.
[36] D. A. Tamalge and P. J. Curran, "Remote sensing using partially polarized light," *Int. J. Remote Sensing*, vol. 7, pp. 47–64, 1986.
[37] D. Tanré, M. Herman, and P. Y. Deschamps, "Influence of the atmosphere upon space measurements of directional properties," *Appl. Opt.*, vol. 22, pp. 733–741, 1983.
[38] O. B. Toon, J. B. Pollack, B. N. Khare, "The optical constants of several atmospheric aerosol species: Ammonium sulfate, aluminum oxide, and sodium chloride," *J. Geophys. Res.*, vol. 81, pp. 5733–5748, 1976.
[39] L. D. Travis, "EOSP: Earth Observing Scanning Polarimeter," in G. Asrar and D. J. Dokken Eds., *EOS Reference Handbook*. Washington DC: NASA, 1993, pp. 74–75.
[40] V. C. Vanderbilt and L. Grant, "Plant canopy specular reflectance model," *IEEE Trans. Geosc. Remote Sensing*, vol. 23, pp. 722–730, 1985.
[41] V. C. Vanderbilt, L. Grant, L. L. Biehl, and B. F. Robinson, "Specular, diffuse, and polarized light scattered by two wheat canopies," *Appl. Opt.*, 24, pp. 2408–2418, 1985.
[42] V. C. Vanderbilt and K. J. de Venecia, "Specular, diffuse, and polarized imagery of an oat canopy," *IEEE Trans. Geosci. Remote Sensing*, vol. GRS–26, pp. 451–462, 1988.
[43] P. Woessner and B. Hapke, "Polarization of light scattered by clover," *Remote Sensing Env.*, vol. 21, pp. 243–261, 1987.
[44] M. Wolff, "Polarization of light reflected from rough planetary surface," *Appl. Opt.*, vol. 14, pp. 1395–1405, 1975.

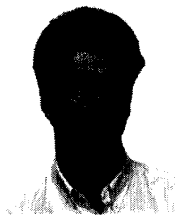

Francois-Marie Bréon received the M.S. and Ph.D. degrees in physics from the Université de Paris, Paris, France, in 1986 and 1989, respectively.

After completing a postgraduate position at the Scripps Institution of Oceanography, University of California, San Diego, he joined the POLDER science team in 1991, where he conducts research in atmospheric radiative transfer theory and developing satellite data inversion algorithms for both the solar and infrared spectral domains. He is currently a Project Scientist for the POLDER ground segment and a Researcher at the Laboratoire de Modélisation du Climat et de l'Environnement, Saclay, France. His research interests include investigating terrestrial processes and climate change using satellite remote sensing techniques to retrieve important terrestrial parameters.

Didier Tanré received the M.Sc. degree in physics and the "These de 3eme Cycle," and "Doctorat d'Etat" degrees in atmospheric physics from the Universite des Sciences et Techniques de Lille, France, in 1975, 1977, and 1982, respectively.

He is an Atmospheric Scientist in the CNRS, colocated with the Laboratoire d'Optique Atmospherique at the Université des Sciences et Techniques, where he has been a Research Scientist since 1982. He has been a member of the MODIS science teams since 1989. In addition, he was an NRC Resident Research Associate at NASA Goddard Space Flight Center from 1989 to 1991. His research experience includes radiative transfer modeling through realistic atmospheres, both theory and applications. His interests also include remote sensing of atmospheric properties from satellite and ground-based observations as well as atmospheric effects in satellite imagery of the earth's surface.

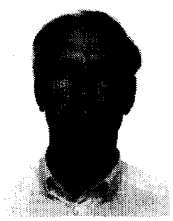

Pierre Lecomte received the M.S. degree in applied physics from Lille University, Lille, France, in 1966.

His work has focused on the radiative transfer in the ocean-atmoshperic system. He has been with the Laboratoire d'Optique Atmosphérique, Lille, France, working on scientific instrumentation development and test.

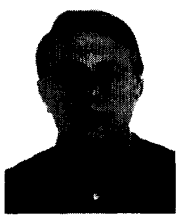

Maurice Herman received the M.S. and Ph.D. degrees in physics from the Université de Lille, Lille, France, in 1962 and 1968, respectively.

He is currently a Professor of Physics at the Université de Lille, and the Director of the Laboratoire d'Optique Atmosphérique. His research activities include radiative transfer theory and atmospheric signal modeling, planetary atmosphere studies that employ telescopic observations, and aerosols studies using ground-based and balloon-borne instruments that exploit the information content of polarization data. He is one of the original architects of the POLDER project, and he is involved in the inversion retrievals of aerosol properties from POLDER instrument measurements.